Continuum Mech. Thermodyn. (2000) 12: 195–216

Full and reduced model solutions of steady axi-symmetric ice sheet flow over small and large bed topography slopes

K.A. Cliffe[1], **L.W. Morland**[2]

[1] AEA Technology plc, 424.4 Harwell, Didcot, Oxfordshire OX11 0RA, UK
[2] School of Mathematics, University of East Anglia, Norwich NR4 7TJ, UK

Received September 10, 1999

Two numerical methods for solving the full steady ice-sheet equations in axi-symmetric flow are described. The free-boundary problem is treated by transforming the problem to a fixed domain using either an orthogonal co-ordinate transformation or a variant of a transformation proposed by Landau, and difficulties with the former, more sophisticated, method are demonstrated. The simpler *Reduced Model* is also presented, and accurate solutions for flows over bed topography with moderate to large slopes are generated by an inverse method for comparison with the numerical solutions of the full equations. The reduced model is not valid for such bed slopes, and the comparisons demonstrate the extent and nature of the errors arising from the use of the simpler model.

1 Introduction

Ice-sheet evolution in response to climate change is of interest in the contex of global warming and also because of the potential impact of ice sheets on the performance of repositories for long-lived radioactive waste. Simulations of ice-sheet evolution hinge on large scale numerical computation. Model equations must incorporate a sound physical description of the response of ice to stress and temperature, and the mechanical and thermal interactions at the surface and base with the atmosphere and bed, which lead to a complex initial/boundary value problem on the unknown ice-sheet domain. Current treatments assume that the ice is an incompressible non-linearly viscous fluid with a temperature dependent rate factor which gives rise to strong thermo-mechanical coupling through heat advection in the energy balance. A detailed review of current practice is given by Morland (1993). In particular, all large-scale numerical treatments are based on the *Reduced Model* which is derived from the leading order balances and relations in an asymptotic expansion in a small parameter ϵ. This can be introduced as the ratio of a thickness magnitude to a span magnitude, equivalently the ratio of a vertical velocity magnitude to a horizontal velocity magnitude, which is the basis of Hutter's (1983) *Shallow Ice Approximation*, or alternatively as a dimensionless viscous parameter defined by the momentum balance, which emerged in the formulations developed by Morland and Johnson (1980, 1982), Morland and Smith (1984) and Morland (1984, 1993). An essential feature of the asymptotic expansion is that gradients in longitudinal directions are small compared to those through the thickness, in the ratio ϵ, which leads to a surface slope of order ϵ. The asymptotic validity formally requires that basal conditions must not induce longitudinal gradients greater than order ϵ, so that, in particular, slopes of the bed topography must not exceed order ϵ. The *Reduced Model*, then, is formally valid only when bed topography slopes are extremely small. In reality, the beds of the large ice sheets, such as the present Antarctic and Greenland ice sheets, have topographies with significant slopes, and application of the *Reduced Model* must be questioned.

The large mesh spacings currently adopted for practical considerations in the large-scale numerical simulations are unable to resolve rapidly varying topographic features, and in any case cannot represent the

associated large gradients, so the effects of real topography are lost. A series of European Ice Sheet Modelling Initiative Workshops on Model Intercomparisons (Brussels, 1993; Bremerhaven, 1994; Grindelwald, 1997), the first two reported by Huybrechts and Paynes (1996), presented comparisons between solutions to idealised test problems obtained by different, but related, numerical algorithms applied to the *Reduced Model* equations. While there was general agreement on the ice-sheet profiles, significant differences in the temperature fields emerged, which in turn must influence the flow through the strong thermo-mechanical coupling. Comparisons with known accurate *Reduced Model* solutions for low slope beds had not been performed. The present study obtains numerical solutions of the full equations for steady axi-symmetric flow under prescribed isothermal and non-uniform temperature fields, for a variety of basal conditions, and compares these with accurate solutions to the corresponding *Reduced Model*, to demonstrate the nature and extent of the differences. Such differences could be enhanced by the strong thermo-mechanical coupling when the energy balance is included, but these first comparisons focus on the basic distinctions in steady uncoupled flow to show the effects of simply neglecting longitudinal gradients, highlight the numerical difficulties of solving the full model equations and illustrate a new approach to resolving those difficulties.

The full three-dimensional model equations are stated in appropriate non-dimensional variables. Then the equations for steady axi-symmetric flow are derived, and their leading order relations which describe the *Reduced Model*. Exact *Reduced Model* solutions for moderate and finite slope topography are constructed by inverse methods for comparisons with solutions to the full equations. Two co-ordinate mapping techniques to transform the problem to a fixed domain are described, an orthogonal mapping and a variant on a Landau transformation. The finite element solution procedure is presented, and the accuracy of the basic algorithm is tested by comparison with flat bed *Reduced Model* solutions which have errors of order ϵ^2. Features of the two mapping techniques are discussed: a failure of the orthogonal mapping, and, in the Landau approach, the need to apply the surface kinematic condition in the appropriate manner. Numerical solutions for the full governing equations for ice-sheet flow have been obtained previously by Mangeney et al. (1997) using a finite-difference method.

The major results are the final comparisons of a variety of full and *Reduced Model* solutions for different bed topography features, which show that the predicted sheet profiles are very similar, in these examples, but velocity fields have significant differences in zones extending to the surface above bed sections containing appreciable topography. Such differences must influence the heat advection when the energy balance is considered, and in turn the viscous response through the strong temperature dependence, so the coupled theory can be expected to yield larger differences.

2 Governing equations

Ice-sheet dynamics are described by very slow, gravity driven, flow of an incompressible non-linearly viscous fluid with a temperature dependent rate factor. Inertia terms are extremely small, so that the momentum balance is simply equilibrium under gravity, where the gravity acceleration $\boldsymbol{g}$ has vertical component $g = 9.81\,m\,s^{-1}$. Ice density is $\rho = 918\,kg\,m^{-3}$. The maximum temperature range would be $213\,K$ at the surface of a large cold sheet to melting $273\,K$ at a warm base, and over this range it is supposed that the thermal conductivity $\lambda = 2.2\,N\,K^{-1}s^{-1}$ and specific heat $C = 2 \times 10^3 N\,m\,kg^{-1}K^{-1}$ are constants. Energy balance for cold ice, with no internal melting, is approximated by the balance between local heating and heat advection with heat diffusion and stress working, though the latter is negligible except perhaps in a warm basal boundary layer. Details of the formulation and following model equations are presented in Morland (1993).

It is convenient to present all the relations in appropriate dimensionless variables from the outset. In spatial co-ordinates, a position vector $\boldsymbol{r}$ and its length co-ordinates have unit d_0, which is the ice-sheet thickness magnitude, the velocity $\boldsymbol{u}$ and its components have unit q_0, which is the magnitude of the surface accumulation or basal melt: volume of ice entering/leaving the sheet per unit area per unit time. The time t has unit d_0/q_0, and the strain-rate $\boldsymbol{D}$ has unit q_0/d_0. The stress $\boldsymbol{\sigma}$ has unit $\rho g\,d_0$, which is the magnitude of the overburden pressure at depth d_0. A normalised dimensionless temperature $\bar{T}$ is defined in terms of the temperature T by

$$T = T_0 + \Delta_T\,\bar{T}\,, \quad \Delta_T = 20\,K\,, \quad T_0 = 273\,K\,, \tag{2.1}$$

where T_0 is the (approximate) melt temperature. The mass, momentum and energy balances are now

$$\nabla . \boldsymbol{u} = \mathbf{0} \ , \tag{2.2}$$

$$\nabla . \boldsymbol{\sigma} + \rho \mathbf{g} = \mathbf{0} \ , \tag{2.3}$$

$$\frac{\partial \bar{T}}{\partial t} + \boldsymbol{u} . \nabla \bar{T} = k \nabla^2 \bar{T} + \alpha \, tr \, [\boldsymbol{\sigma D}] \ , \tag{2.4}$$

where

$$k = \frac{\lambda}{\rho C \, d_0 \, q_0} \ , \quad \alpha = \frac{g \, d_0}{C \, \Delta_T} \ , \quad \boldsymbol{D} = \frac{1}{2} (\nabla \boldsymbol{u} + [\nabla \boldsymbol{u}]^T) \ , \tag{2.5}$$

and the spatial gradients are with respect to the dimensionless co-ordinates.

The commonly adopted viscous shear law is the simplified relation in which deviatoric stress and strain-rate are parallel, with the non-linear dependence on just the second principal invariant of the deviatoric stress or of the strain-rate, and temperature dependence is through a rate factor $a(\bar{T})$. In the above dimensionless variables this takes the equivalent forms

$$\boldsymbol{D} = \epsilon^{-2} \, \bar{a}(\bar{T}) \, \psi(J) \, \hat{\boldsymbol{\sigma}} \ , \quad \hat{\boldsymbol{\sigma}} = \epsilon^2 \, \bar{a}^{-1}(\bar{T}) \, \phi(I) \, \boldsymbol{D} \ , \tag{2.6}$$

where the deviatoric stress $\hat{\sigma}$ is defined in terms of the stress $\boldsymbol{\sigma}$ and mean pressure p by

$$\hat{\boldsymbol{\sigma}} = \boldsymbol{\sigma} + p \, \boldsymbol{I} \ , \quad p = -\frac{1}{3} \, tr \, \boldsymbol{\sigma} \ , \tag{2.7}$$

where $\boldsymbol{I}$ is the unit tensor, and $a(\bar{T}) = a_0 \, \bar{a}(\bar{T})$ where $a_0 = a(0)$ is the rate factor at temperature T_0. The dimensionless parameter ϵ is defined by

$$\epsilon^2 = \frac{\sigma_0 q_0}{\rho g d_0^2 D_0 a_0} \ , \tag{2.8}$$

where the shear-stress and strain-rate units, σ_0 and D_0 respectively, are chosen to normalise the response functions $\psi(J)$ and $\phi(I)$, so that ϵ^2 is the magnitude of a dimensionless viscosity in the stress law $(2.6)_2$. The arguments J and I are defined by

$$J = \frac{1}{2} \, \vartheta \, \epsilon^{-2} \, tr \, \hat{\sigma}^2 \ , \quad I = \frac{1}{2} \, \vartheta \, \epsilon^2 \, \bar{a}^{-2}(\bar{T}) \, tr \boldsymbol{D}^2 \ , \quad \vartheta = \frac{\rho g q_0}{\sigma_0 D_0 a_0} \ . \tag{2.9}$$

It will be seen that ϵ is very small for typical ice-sheet parameters, and is the small parameter referred to in the Introduction which defines the ice-sheet aspect ratio. The *Reduced Model* is based on the leading order balances in an asymptotic expansion in ϵ.

Smith and Morland (1981) have determined an accurate polynomial representation for $\psi(J)$ based on Glen's (1955) experimental data at temperature $T_0 = 273.15 \, K$:

$$a_0 \psi(J) = 0.3336 + 0.32 \, J + 0.0296 \, J^2 \ , \tag{2.10}$$

with the normalising parameters

$$D_0 = 3.18 \times 10^{-8} \mathrm{s}^{-1} \ , \quad \sigma_0 = 10^5 \mathrm{Nm}^{-1} \ . \tag{2.11}$$

Direct application of the momentum equation (2.3) requires the law for $\hat{\boldsymbol{\sigma}}$, that is, $\phi(I)$. The equivalence of the two forms (2.6) yields the relations

$$\phi(I) \psi(J) = 1 \ , \quad J = I \phi^2(I) \ \rightarrow \ \phi(I) \psi[I \phi^2(I)] = 1 \ , \tag{2.12}$$

and the latter determines a unique $\phi(I)$ when $\psi(J)$ is a prescribed monotonic function. The rate factor determined by Smith and Morland (1981) from Mellor and Testa's laboratory data over a temperature range $212 \, K$–$273 \, K$ is

$$\bar{a}(\bar{T}) = 0.68 \exp(12 \bar{T}) + 0.32 \exp(3 \bar{T}) \ , \quad a_0 = 1 \, . \tag{2.13}$$

Note the decrease of $\bar{a}(\bar{T})$ from 1 at $273 \, K$ to 1.6×10^{-2} at $253 \, K$ to 7.9×10^{-4} at $233 \, K$, which shows the strong influence of temperature on the viscous response. A choice of a_0 less than unity would model ice

which is stiffer than the laboratory sample. The relations (2.10) and (2.13) are adopted for the applications in this study.

Boundary conditions are prescribed on the unknown ice-sheet surface and the given bed, and in the case of axial symmetry the surface and bed slope on the axis are zero, and the radial velocity is zero. The surface $\mathscr{S}$ and its unit outward normal $\boldsymbol{n}$ can be defined by

$$\mathscr{S}: \quad S(\boldsymbol{r},t) = 0\,, \quad \boldsymbol{n} = \nabla S/|\nabla S|\,. \tag{2.14}$$

Let the stress be measured relative to an assumed uniform atmospheric pressure, then the surface is traction free:

$$\mathscr{S}: \quad \boldsymbol{\sigma}.\boldsymbol{n} = \boldsymbol{0}\,. \tag{2.15}$$

If the accumulation – the volume of ice entering the sheet per unit surface area per unit time – is q_n, negative where ablation occurs, then the surface kinematic condition is

$$\mathscr{S}: \quad \frac{\partial S}{\partial t} + \boldsymbol{u}.\nabla S = -|\nabla S|\, q_n\,, \tag{2.16}$$

which is the additional boundary condition required to determine the surface position. A common thermal condition is the prescription of the surface temperature:

$$\mathscr{S}: \quad T = T_s\,, \tag{2.17}$$

which could be a function of elevation and horizontal location.

While the bed of an ice sheet will rise and fall as the sheet thins and thickens, with time lags, the present comparisons are made for a fixed bed:

$$\mathscr{B}: \quad B(\boldsymbol{r}) = 0\,, \quad \boldsymbol{n} = \nabla B/|\nabla B|\,, \tag{2.18}$$

with unit outward normal $\boldsymbol{n}$. Let b_n be the basal melt – the volume of ice leaving the sheet per unit bed area per unit time – negative where refreezing occurs, then the bed kinematic condition is

$$\mathscr{B}: \quad \boldsymbol{u}.\nabla B = |\nabla B|\, b_n\,. \tag{2.19}$$

It is common to assume a sliding law which relates the tangential traction to the tangential slip velocity, with a coefficient depending on the normal pressure. In particular, Morland and Johnson (1980) show that the coefficient must be proportional to the pressure, as the pressure (sheet thickness) approaches zero, to eliminate a surface slope singularity at a margin in the *Reduced Model*. For the present illustrations a sliding law linear in velocity and normal pressure is adopted:

$$\mathscr{B}: \quad \boldsymbol{s}.\boldsymbol{\sigma}.\boldsymbol{n} = -\epsilon^2\, \Lambda\, (\boldsymbol{n}.\boldsymbol{\sigma}.\boldsymbol{n})\, \boldsymbol{u}.\boldsymbol{s}\,, \tag{2.20}$$

where $\boldsymbol{s}$ is any unit tangent vector; this implies that the tangential traction and slip velocity are parallel. The factor ϵ^2 is introduced to ensure that the slip velocity does not exceed the surface velocity in a flat bed *Reduced Model* solution when the friction coefficient Λ is order unity or greater; bed topography will not change the interface friction conditions. As Λ increases the slip velocity decreases, for given traction, and the limit condition of no-slip corresponds to infinite Λ:

$$\mathscr{B}: \quad \boldsymbol{u}.\boldsymbol{s} = 0 \quad \text{(no-slip)}\,. \tag{2.21}$$

The thermal condition could be an energy jump condition involving the latent heat associated with melting or freezing, but a more common simpler prescription is the balance with a geothermal heat flux $\boldsymbol{G}$:

$$\lambda\, \boldsymbol{n}.\nabla T = -\boldsymbol{G}.\boldsymbol{n}\,. \tag{2.22}$$

3 Axi-symmetric steady flow

A detailed analysis of radially symmetric flow and the derivation of a reduced model is presented by Morland (1997), where solutions for the prescribed temperature theory are also constructed. Hutter et al. (1987) obtained direct numerical solutions for the coupled balances of steady radially symmetric flow and showed the influence of different boundary conditions. This outline provides a self-contained formulation, in the dimensionless variables intoduced in the previous section, of the boundary value problems addressed in this study for steady axi-symmetric flow.

Steady axi-symmetric flow of a large ice sheet is described by radial and vertical velocity fields $u(r,z)$ and $w(r,z)$ respectively, where (r,θ,z) are cylindrical polar co-ordinates with z vertically upward, and the flow variables are independent of the polar angle θ. The corresponding non-zero dimensionless physical components of the strain-rate are

$$D_{rr} = \frac{\partial u}{\partial r}\,, \quad D_{\theta\theta} = \frac{u}{r}\,, \quad D_{zz} = \frac{\partial w}{\partial z}\,, \quad D_{rz} = \frac{1}{2}\left(\frac{\partial u}{\partial z} + \frac{\partial w}{\partial r}\right), \tag{3.1}$$

subject to the incompressibility, mass balance, condition

$$\frac{\partial u}{\partial r} + \frac{u}{r} + \frac{\partial w}{\partial z} = 0\ , \tag{3.2}$$

which is satisfied identically by expressing the velocity components in terms of a stream function $\omega(r,z)$:

$$u = \frac{1}{r}\frac{\partial \omega}{\partial z}\,, \quad w = -\frac{1}{r}\frac{\partial \omega}{\partial r}\,. \tag{3.3}$$

The non-zero dimensionless physical components of stress are σ_{rr}, $\sigma_{\theta\theta}$, σ_{zz} and σ_{rz}, with associated deviatoric stresses

$$\hat\sigma_{rr} = \sigma_{rr} + p\,, \quad \hat\sigma_{\theta\theta} = \sigma_{\theta\theta} + p\,, \quad \hat\sigma_{zz} = \sigma_{zz} + p\,, \quad \hat\sigma_{rz} = \sigma_{rz}\,. \tag{3.4}$$

The horizontal radial and vertical momentum balances for this very slow flow are

$$-\frac{\partial p}{\partial r} + \frac{\partial \hat\sigma_{rr}}{\partial r} + \frac{\hat\sigma_{rr} - \hat\sigma_{\theta\theta}}{r} + \frac{\partial \hat\sigma_{rz}}{\partial z} = 0\,, \quad -\frac{\partial p}{\partial z} + \frac{\partial \hat\sigma_{zz}}{\partial z} + \frac{\partial \hat\sigma_{rz}}{\partial r} + \frac{\hat\sigma_{rz}}{r} - 1 = 0\,, \tag{3.5}$$

and the circumferential balance is automatically satisfied.

The deviatoric viscous law $(2.6)_2$ has the non-zero components

$$\hat\sigma_{rr} = 2\epsilon^2\mu\frac{\partial u}{\partial r}\ , \quad \hat\sigma_{\theta\theta} = 2\epsilon^2\mu\frac{u}{r}\ , \quad \hat\sigma_{zz} = 2\epsilon^2\mu\frac{\partial w}{\partial z}\ , \quad \hat\sigma_{rz} = \epsilon^2\mu\left(\frac{\partial u}{\partial z} + \frac{\partial w}{\partial r}\right)\ , \tag{3.6}$$

where μ is given by

$$\mu = \frac{1}{2}\,a^{-1}(T)\,\phi(I) = \frac{1}{2}\,a^{-1}(T)\,\psi^{-1}(J)\,. \tag{3.7}$$

Now the factor $\epsilon^2 a^{-1}(T)$ which is a measure of the dimensionless viscosity is highly non-uniform when temperature varies over $20K$ or more, and for thin sheets with very cold surfaces, when ϵ is not too small and a at the surface is small, this factor can approach order unity near the surface. For simplicity, the order of magnitude arguments presented in the next section to derive the *Reduced Model* assume this factor is small, of order ϵ^2 as in the original Morland and Johnson (1980) isothermal treatment with $a_0 = 1$. An analysis allowing for non-uniformity with large temperature variation was presented by Morland (1984), and again more elaborately by Morland (1993), to yield the same leading order reduced model, with the assumption that the base is close to the temperature T_0. An isothermal approximation at a colder temperature T_c should therefore set $\bar a(\bar T) = 1$ and choose $a_0 = a(T_c)$ in the definition (2.8) of ϵ, which then increases as T_c decreases.

The traction-free surface $z = h(r)$ is subjected to a normal ice flux q_n, which is positive over accumulation zones and negative over ablation zones. It is expected that accumulation will occur over a central zone at higher elevations and ablation below a snow line. A simple dependence of q_n on elevation h is a common prescription, but dependence only on r allows a simpler solution. Let the surface have unit tangent and outward normal vectors $\boldsymbol{s}$ and $\boldsymbol{n}$ in a right-hand sense, then

$$\boldsymbol{n} = \Delta_h^{-1}\,[-h'(r), 0, 1]\ , \quad \boldsymbol{s} = \Delta_h^{-1}\,[1, 0, h'(r)]\ , \quad \Delta_h = \left\{1 + [h'(r)]^2\right\}^{\frac{1}{2}}\ . \tag{3.8}$$

The zero traction is conveniently expressed in terms of vanishing normal and tangential tractions $t_n = \boldsymbol{n}.\boldsymbol{\sigma}.\boldsymbol{n}$ and $t_s = \boldsymbol{s}.\boldsymbol{\sigma}.\boldsymbol{n}$ in the Orz plane:

$$z = h(r): \quad \Delta_h^2\, t_n = -\Delta_h^2\, p + \hat{\sigma}_{zz} + [h'(r)]^2\,\hat{\sigma}_{rr} - 2\,h'(r)\,\hat{\sigma}_{rz} = 0\,, \tag{3.9}$$

$$z = h(r): \quad \Delta_h^2\, t_s = \left\{1 - [h'(r)]^2\right\}\,\hat{\sigma}_{rz} + h'(r)\,(\hat{\sigma}_{rr} - \hat{\sigma}_{zz}) = 0\,. \tag{3.10}$$

The kinematic condition (2.16) prescribing the surface accumulation flux becomes

$$z = h(r): \quad -\Delta_h\, v_n = h'(r)\,u - w = \Delta_h\, q_n = \tilde{q}\,, \tag{3.11}$$

where v_n is the normal velocity and $\tilde{q}$ is the equivalent vertical flux which can be identified with equivalent vertical snow fall. This is the additional boundary condition required to determine the unknown surface $h(r)$.

The bed $z = f(r)$ is prescribed. Unit tangent and outward normal vectors $\boldsymbol{s}$ and $\boldsymbol{n}$ in a right-hand sense are defined by

$$\boldsymbol{n} = \Delta_f^{-1}\,[f'(r), 0, -1]\ , \quad \boldsymbol{s} = \Delta_f^{-1}\,[-1, 0, -f'(r)]\ , \quad \Delta_f = \left\{1 + [f'(r)]^2\right\}^{\frac{1}{2}}\ . \tag{3.12}$$

Normal and tangential tractions t_n and t_s are given by

$$z = f(r): \quad \Delta_f^2\, t_n = -\Delta_f^2\, p + \hat{\sigma}_{zz} + [f'(r)]^2\hat{\sigma}_{rr} - 2\,f'(r)\,\hat{\sigma}_{rz}\ , \tag{3.13}$$

$$z = f(r): \quad \Delta_f^2\, t_s = \left\{1 - [f'(r)]^2\right\}\,\hat{\sigma}_{rz} + f'(r)\,(\hat{\sigma}_{zz} - \hat{\sigma}_{rr})\ , \tag{3.14}$$

and normal and tangential velocities v_n and v_s by

$$z = f(r): \quad \Delta_f\, v_n = f'(r)\,u - w\ , \tag{3.15}$$

$$z = f(r): \quad \Delta_f\, v_s = -u - f'(r)\,w\ . \tag{3.16}$$

The kinematic condition (2.19) prescribing the normal basal melt flux b_n, negative if freezing occurs, becomes

$$z = f(r): \quad \Delta_f\, v_n = f'(r)\,u - w = \Delta_f\, b_n = \tilde{b}\ , \tag{3.17}$$

where $\tilde{b}$ is an equivalent vertical flux. The linear sliding relation (2.20) between the tangential traction and velocity becomes

$$z = f(r): \quad t_s = \epsilon^2\,\Lambda\, t_n\, v_s\ , \tag{3.18}$$

where Λ is an order unity or greater constant friction coefficient. A special simpler case is that of no-melt/freezing and no-slip:

$$z = f(r): \quad v_n = v_s = 0 \rightarrow u = w = 0\,. \tag{3.19}$$

The no-slip condition gives rise to unbounded surface slope at a margin at which there is ablation in the reduced model, which violates the expansion scheme.

4 Reduced model

With the assumption that $\bar{a}$, and hence μ, is order unity, it is evident from the deviatoric stress expressions (3.6) that they are small compared to the order unity pressure, given that the vertical and horizontal strain-rates are order unity, or, at least, much smaller than ϵ^{-2}, so the zero surface normal traction (3.9) implies that the pressure p vanishes at order unity at the surface $z = h(r)$. The vertical equilibrium $(3.5)_2$ then implies that at order unity $p = -z + h(r)$. Now the horizontal equilibrium $(3.5)_1$ would imply that $h(r)$ is constant at order unity, so that the surface could not return to the bed at a finite margin span, unless there is a deviatoric stress gradient sufficiently large to balance a non-zero horizontal pressure gradient. A finite span sheet therefore requires that the vertical gradient of $\hat{\sigma}_{rz}$ provides the balance, which is reflected by the co-ordinate stretching and variable scalings

$$R = \epsilon\, r\ , \quad Z = z\ , \quad H(R) = h(r)\ , \quad F(R) = f(r)\ , \tag{4.1}$$

$$U(R,Z) = \epsilon\, u(r,z) \ , \quad W(R,Z) = w(r,z) \ , \quad P(R,Z) = p(r,z) \ , \tag{4.2}$$

$$\hat{\sigma}_{rz} = \epsilon\, \hat{\Sigma}_{rz} \ , \quad \hat{\sigma}_{rr} = \epsilon^2\, \hat{\Sigma}_{rr}, \quad \hat{\sigma}_{\theta\theta} = \epsilon^2\, \hat{\Sigma}_{\theta\theta} \ , \quad \hat{\sigma}_{zz} = \epsilon^2\, \hat{\Sigma}_{zz} \ , \tag{4.3}$$

where the capital symbols are order unity and R and Z derivatives have equal status. The mass balance, incompressibility, condition (3.2) is now expressed by

$$\Omega(R,Z) = \epsilon^2\, \omega(r,z) \ , \quad U = \frac{1}{R}\frac{\partial \Omega}{\partial Z} \ , \quad W = -\frac{1}{R}\frac{\partial \Omega}{\partial R} \ , \tag{4.4}$$

and the viscous relations (3.6) become

$$\hat{\Sigma}_{rr} = 2\,\mu \left(\frac{1}{R}\frac{\partial^2 \Omega}{\partial R \partial Z} - \frac{1}{R^2}\frac{\partial \Omega}{\partial Z} \right) \ , \qquad \hat{\Sigma}_{\theta\theta} = 2\,\mu\, \frac{1}{R^2}\frac{\partial \Omega}{\partial Z} \ , \quad \hat{\Sigma}_{zz} = -2\,\mu\, \frac{1}{R}\frac{\partial^2 \Omega}{\partial R \partial Z} \ ,$$

$$\hat{\Sigma}_{rz} = \mu \left(\frac{1}{R}\frac{\partial^2 \Omega}{\partial Z^2} - \epsilon^2\, \frac{1}{R}\frac{\partial^2 \Omega}{\partial R^2} + \epsilon^2\, \frac{1}{R^2}\frac{\partial \Omega}{\partial R} \right) \ , \tag{4.5}$$

where the invariants J and I defined by (2.9), appearing in the expression (3.7) for μ, are given by

$$J = \vartheta \left[\hat{\Sigma}_{rz}^2 + \epsilon^2 \left(\hat{\Sigma}_{rr}^2 + \hat{\Sigma}_{rr}\hat{\Sigma}_{zz} + \hat{\Sigma}_{zz}^2 \right) \right] \ , \tag{4.6}$$

$$\begin{aligned} I \ = \ & \vartheta \bar{a}^{-2} \\ & \times \left[\frac{1}{4} \left(\frac{\partial U}{\partial Z} \right)^2 + \epsilon^2 \left\{ \left(\frac{\partial U}{\partial R} \right)^2 + \frac{\partial U}{\partial R}\frac{\partial W}{\partial Z} + \left(\frac{\partial W}{\partial Z} \right)^2 + \frac{1}{2}\frac{\partial U}{\partial Z}\frac{\partial W}{\partial R} \right\} \right. \\ & \left. + \frac{1}{4}\epsilon^4 \left(\frac{\partial W}{\partial R} \right)^2 \right] . \end{aligned} \tag{4.7}$$

The surface slope is of order ϵ, expressed by

$$h'(r) = \epsilon\, H'(R) = \epsilon\, \Gamma(R) \ , \tag{4.8}$$

so that the ice-sheet span is of order ϵ^{-1}. It is formally assumed that both R and Z derivatives of the normalised capital variables do not exceed unity in magnitude, and in particular Γ does not exceed unity in magnitude. It is seen later how this restricts permitted bed slopes.

The momentum balances (3.5) now become

$$-\frac{\partial P}{\partial R} + \epsilon^2 \frac{\partial \hat{\Sigma}_{rr}}{\partial R} + \epsilon^2\, \frac{\hat{\Sigma}_{rr} - \hat{\Sigma}_{\theta\theta}}{R} + \frac{\partial \hat{\Sigma}_{rz}}{\partial Z} \ = \ 0 \ , \tag{4.9}$$

$$-\frac{\partial P}{\partial Z} + \epsilon^2 \frac{\partial \hat{\Sigma}_{zz}}{\partial Z} + \epsilon^2 \frac{\partial \hat{\Sigma}_{rz}}{\partial R} + \epsilon^2\, \frac{\hat{\Sigma}_{rz}}{R} - 1 \ = \ 0 \ , \tag{4.10}$$

which, neglecting terms of order ϵ^2 compared to unity, give the leading order balances

$$\frac{\partial P}{\partial Z} = -1 \ , \quad \frac{\partial P}{\partial R} = \frac{\partial \hat{\Sigma}_{rz}}{\partial Z} = \mu\, \frac{1}{R}\frac{\partial^3 \Omega}{\partial Z^3} \ , \tag{4.11}$$

while the surface traction conditions (3.9) and (3.10) require to leading order,

$$Z = H(R): \quad P = 0 \ , \quad \Sigma_{rz} = 0 \ . \tag{4.12}$$

Integrating the vertical equilibrium equation $(4.11)_1$ subject to the surface pressure condition $(4.12)_1$ determines the leading order expressions

$$Z = H(R) = H_0(R), \quad P = P_0(R,Z) = H_0(R) - Z \ . \tag{4.13}$$

The horizontal equilibrium equation $(4.11)_2$ and the surface tangential traction condition $(4.12)_2$ now have the leading order expressions

$$\Omega = \Omega_0(R,Z) \ , \quad H_0'(R) = \Gamma_0(R) = \frac{\partial \Sigma_{rz}^0}{\partial Z} = \mu \, \frac{1}{R} \, \frac{\partial^3 \Omega_0}{\partial Z^3} \ , \tag{4.14}$$

$$Z = H_0(R): \quad \frac{\partial^2 \Omega_0}{\partial Z^2} = 0 \ . \tag{4.15}$$

Integrating $(4.14)_2$ subject to the surface traction condition (4.15) then gives the leading order vertical shear stress and stream function gradient

$$\Sigma_{rz}^0(R,Z) = \mu \, \frac{1}{R} \, \frac{\partial^2 \Omega_0}{\partial Z^2} = -\Gamma_0(R)\,[H_0(R) - Z] \ . \tag{4.16}$$

From the viscous relation $(3.6)_4$ with (3.7) and the leading order shear stress expression (4.16) and velocity gradient $(3.6)_2$, to leading order

$$\frac{\partial U_0}{\partial Z} = \frac{1}{R} \, \frac{\partial^2 \Omega_0}{\partial Z^2} = 2\, a(T) \psi(J)\, \Sigma_{rz}^0 \ , \quad J = \vartheta\,[\Sigma_{rz}^0]^2 = \vartheta\, \Gamma_0^2(R)\,[H_0(R) - Z]^2 \, , \tag{4.17}$$

which can be expressed as

$$\frac{\partial U_0}{\partial Z} = \frac{1}{R} \, \frac{\partial^2 \Omega_0}{\partial Z^2} = \zeta\, a(T) g(\tau) \ , \quad \zeta = -\mathrm{sgn}\,(\Gamma_0) \ , \tag{4.18}$$

where

$$\tau = -\zeta\, \Gamma_0(R)\,[H_0(R) - Z] \geq 0 \ , \quad g(\tau) = 2\tau\, \psi(\vartheta\, \tau^2) \geq 0 \ . \tag{4.19}$$

To leading order, $\Delta_h = 1$, $q_n[R, H(R)] = \tilde{q}[R, H_0(R)]$, and the kinematic condition (3.11) becomes

$$\begin{aligned} Z = H_0(R): \quad -v_n &= \Gamma_0(R)\, U_0[R, H_0(R)] - W_0[R, H_0(R)] \\ &= \frac{1}{R} \, \frac{d}{dR} \, \Omega_0[R, H_0(R)] = \tilde{q}[R, H_0(R)] \ . \end{aligned} \tag{4.20}$$

For a prescribed temperature field $T(R,Z)$, uncoupled from the energy balance, the rate factor $a(T)$ becomes a known function of (R,Z). Define

$$g_1(R,Z) = \int_F^Z a(T')\, g(\tau')\, \mathrm{d}Z' \ , \quad T' = T(R,Z') \ , \quad \tau' = -\zeta\, \Gamma_0(R)\,[H_0(R) - Z'] \ , \tag{4.21}$$

$$g_2(R,Z) = \int_F^Z g_1(R,Z')\, \mathrm{d}Z' = \int_F^Z (Z - Z')\, a(T')\, g(\tau')\, \mathrm{d}Z' \ . \tag{4.22}$$

By construction,

$$g_1[R, F(R)] = g_2[R, F(R)] = 0 \ . \tag{4.23}$$

From (4.18), denoting evaluation on the bed $Z = F(R)$ by a subscript $_b$,

$$U_0(R,Z) = U_{0b}(R) + \zeta\, g_1(R,Z) \ , \tag{4.24}$$

$$\Omega_0(R,Z) = \Omega_{0b}(R) + R\, U_{0b}(R)[Z - F(R)] + R\, \zeta\, g_2(R,Z) \ , \tag{4.25}$$

and hence

$$\begin{aligned} W_0(R,Z) \quad = \quad & -\frac{1}{R} \, \frac{d\Omega_{0b}}{dR} - \frac{1}{R}\, U_{0b}(R)[Z - F(R)] + U_{0b}(R) F'(R) \\ & - \frac{dU_{0b}}{dR}\,[Z - F(R)] - \frac{1}{R}\, \zeta\, g_2(R,Z) - \zeta\, \frac{\partial g_2}{\partial R} \ . \end{aligned} \tag{4.26}$$

On the divide $R = 0$, by symmetry Γ_0, τ and U_b^0 are zero, and hence g, g_1 and U are zero. Denoting evaluation on the surface $Z = H_0(R)$ by a subscript $_s$,

$$U_{0s}(R) = U_{0b}(R) + \zeta\, g_1[R, H_0(R)] \ , \tag{4.27}$$

$$\Omega_{0s}(R) = \Omega_{0b}(R) + R\, U_{0b}(R)[H_0(R) - F(R)] + R\, \zeta\, g_2[R, H_0(R)] \ . \tag{4.28}$$

The leading order solution is completed by satisfying the basal melt condition (3.17) and sliding condition (3.18), or non-slip condition, on the bed. With the assumption that the bed slope $f'(r) = \epsilon F'(R)$ is order ϵ or less, then $\Delta_f = 1$ to leading order and (3.17) becomes

$$Z = F(R): \quad F'(R)\, U_{0b}(R) - W_{0b}(R) = \frac{1}{R}\frac{d\,\Omega_{0b}}{dR} = b_n = \tilde{b} \ , \tag{4.29}$$

recalling that $\Omega_{0b}(R) = \Omega_0[R, F(R)]$. The sliding law (3.18), with the leading order values of the tractions (3.13), (3.14), and velocity (3.16), recalling that $\boldsymbol{s}$ points in the negative r direction, becomes

$$Z = F(R): \quad -\Gamma_0(R) = \Lambda\, U_{0b}(R) \ , \tag{4.30}$$

while the no-slip condition is simply

$$Z = F(R): \quad U_{0b} = 0 \ , \tag{4.31}$$

which is obtained from (4.30) by allowing Λ to become infinite. Substituting the expression (4.28) for $\Omega_{0s}(R)$ in the surface kinematic condition (4.20), and eliminating the consequent radial derivative of $\Omega_{0b}(R)$ by (4.29), yields the differential equation

$$\frac{1}{R}\frac{d}{dR}\{R\, U_{0b}(R)[H_0(R) - F(R)] + R\,\zeta\, g_2[R, H_0(R)]\} = \tilde{q} - \tilde{b} = Q[R, H_0(R)] \ . \tag{4.32}$$

With the sliding law (4.30), this becomes the second order differential equation

$$\frac{1}{R}\frac{d}{dR}\left\{-R\,\Lambda^{-1}\Gamma_0(R)[H_0(R) - F(R)] + R\,\zeta\, g_2[R, H_0(R)]\right\} = Q[R, H_0(R)] \tag{4.33}$$

for $H_0(R)$ on an unknown span $0 \le R \le R_M$, subject to the boundary conditions $H_0(R_M) - F(R_M) = 0$ and $\Gamma_0(0) = 0$. For no-slip the U_{0b} term is absent, equivalent to an infinite friction coefficient Λ.

In both cases, provided that, as expected, there is net ablation at the margin, an asymptotic analysis of (4.33) near the margin determines a unique finite surface slope, which depends on R_M, for sliding with finite Λ, and the unique asymptotic behaviour of an unbounded surface slope when there is no-slip at the margin Morland (1997). By (4.21) and (4.22), $g_2[R, H_0(R)] \sim [H_0(R) - F(R)]^3$ as $[H_0(R) - F(R)] \to 0$ when Γ is bounded. For finite Λ, then, the balance in (4.33) as $[H_0(R) - F(R)] \to 0$ is dominated by the linear term associated with sliding. For finite Λ define

$$\Gamma_0(R_M) = \Gamma_M \ , \quad F'(R_M) = \beta_M \ , \qquad Q[R_M, H_0(R_M)] = Q_M < 0 \ , \tag{4.34}$$

then the dominant balance becomes

$$\Gamma_M(\Gamma_M - \beta_M) = -\Lambda\, Q_M \ , \tag{4.35}$$

which has the unique negative slope solution

$$\Gamma_M = \frac{1}{2}(\beta_M - [\beta_M^2 - 4\,\Lambda\, Q_M]^{\frac{1}{2}}) \ , \quad \zeta_M = 1 \ . \tag{4.36}$$

For no-slip, infinite Λ, the balance is necessarily with $g_2[R, H_0(R)]$ which must therefore be linear in $[H_0(R) - F(R)]$ as $[H_0(R) - F(R)] \to 0$, and hence the margin slope is unbounded. Define

$$a(T[R_M, F(R_M)]) = a_M \ , \quad \tau[R_M, F(R_M)] = \tau_M \ , \quad \Delta(R) = H_0(R) - F(R) \ , \tag{4.37}$$

where the thickness $\Delta(R)$ vanishes at the margin R_M, and the tangential traction τ_M at the margin is now non-zero. Since the bed slope at the margin, β_M, is bounded

$$\Delta'(R) \sim H_0'(R), \quad \tau_M \sim -\Delta(R)\,\Delta'(R) = -\frac{1}{2}[\Delta'(R)]^2 , \tag{4.38}$$

and hence the thickness, its gradient and surface slope have the asymptotic behaviours as $R \to R_M$,

$$\Delta(R) \sim (2\,\tau_M)^{\frac{1}{2}}(R_M - R)^{\frac{1}{2}} \ , \quad \Delta'(R) \sim H_0'(R) \sim -(\frac{1}{2}\,\tau_M)^{\frac{1}{2}}(R_M - R)^{-\frac{1}{2}} \ . \tag{4.39}$$

The balance (4.33) now shows, with the substitution $H_0 - Z = \Delta y$, that τ_M is the unique positive root of

$$\tau_M \int_0^1 g(\tau_M y)\,\mathrm{d}y = -Q_M/(2\bar{a}_M) > 0 \ , \tag{4.40}$$

which completes the asymptotic expressions (4.39). In both cases it follows from (4.33) that

$$\int_0^{R_M} R\,Q[R, H_0(R)]\,\mathrm{d}R = 0 \ , \tag{4.41}$$

which states that there is no net flux of ice into the sheet between divide and margin, as required by the steady profile assumption.

Morland (1997) has constructed a variety of solutions for different temperature fields, different accumulation/melt patterns, different bed topographies and different viscous laws, for both sliding and no-slip at the bed. The numerical method is essentially shooting from an assumed margin span R_M with zero thickness there, and either the thickness slope or asymptotic behaviour given by (4.36) or (4.39), and iterating until an R_M is found which yields zero surface slope at the divide $R = 0$. A heat source necessary in the energy balance to determine the prescribed uncoupled temperature field is also constructed. A selection of these solutions has been used to test and confirm the accuracy of the present numerical algorithms for the full equations with a flat or ϵ order slope bed, which in turn are the starting solutions for continuation methods to treat bed profiles with gradually increasing slopes.

5 Reduced model solutions for large bed slopes

In addition to the valid reduced model solutions for bed slopes of order ϵ or less constructed to compare corresponding solutions of the full equations, comparisons with solutions of the reduced differential equation (4.33) when bed slopes are large, including order unity slopes, can test whether applying the reduced model in such cases is satisfactory. In practice, the coarse mesh necessary for a large ice-sheet flow simulation can miss the presence of a large slope over a small span, but even if captured the associated large gradients in a normalised span co-ordinate will result in numerical errors. Furthermore, a reported practice in large scale flow simulations is to identify the tangential traction and velocity with the horizontal components; namely the leading order values when the bed slope does not exceed ϵ. Here this yields the relations (4.29) and (4.30) as the leading order expressions of the kinematic and sliding relations (3.17) and (3.18). Thus, if the bed slope $f'(r)$ has magnitude δ exceeding ϵ, the leading order relations have a local error of order δ^2 instead of ϵ^2 which is the assumption in the conventional reduced model, and will be significant for large bed slopes. This error does not arise in the case of no-slip and no basal melting/refreezing. An improved reduced model to avoid this δ^2 error would retain the exact $f'(r)$ in the basal relations (3.13) – (3.18).

Accurate numerical solution of (4.33), the conventional reduced model, henceforth described simply as the *Reduced Model*, or of an improved form incorporating the bed profile exactly as defined above, will require step lengths in R sufficiently small to represent the variation of the bed profile $F(R)$, which has a derivative of order ϵ^{-1} if the hump amplitude and span are of ice-sheet thickness, and will still be very large for moderately greater spans. However, accurate solutions of (4.33), but not the improved form, can be constructed by inverse methods which avoid numerical representation of derivatives. The solutions of (4.33) constructed for the present comparisons involve only quadrature when the ice is linearly viscous and isothermal, and the net accumulation is prescribed as a function of R only. That is

$$a(T) = \bar{a}_0 \ , \quad g(\tau) = 2\,\psi(0)\,\tau = g_0\,\tau \ , \quad \zeta\, g_2[R, H_0(R)] = -\frac{1}{3}\,\bar{a}_0\, g_0\, \Gamma_0(R)\, \Delta^3(R) \ , \tag{5.1}$$

where g_0 is an order unity constant, $\zeta^2 = 1$, and $\bar{a}_0$ is a constant ranging from 0.2 to 0.016 corresponding to mean temperatures -5K to -20K, and in terms of a normalised radial co-ordinate t,

$$R = R_M\, t \quad (0 \le t \le 1) \ , \quad Q = Q_0\, \tilde{Q}(t) \ , \quad \tilde{Q}(0) = 1 \ . \tag{5.2}$$

With the definitions

$$\Delta = \tilde{\Delta}(t) \ , \quad H_0 = \tilde{H}(t) \ , \quad \Gamma_0 = R_M^{-1}\,\tilde{H}'(t) = R_M^{-1}\,\tilde{\Gamma}(t) \ ,$$
$$\lambda = \frac{1}{3}\,\Lambda\, g_0\,\bar{a}_0 \ , \quad \kappa = 2\,\lambda\,\Lambda\, Q_0\, R_M^2 \ , \quad S(t) = t^{-1}\int_t^1 y\,\tilde{Q}(y)\,\mathrm{d}y \ , \tag{5.3}$$

the differential equation (4.33) and margin condition now becomes a first order differential equation and boundary condition

$$\tilde{\Gamma}(t)\,[\tilde{\Delta}(t) + \lambda\,\tilde{\Delta}^3(t)] = \frac{\kappa}{2\,\lambda}\,S(t) \ , \quad \tilde{\Delta}(1) = 0 \ . \tag{5.4}$$

The integral in (5.3) vanishes at $t = 1$ by (4.41), and with the margin limit $(4.34)_3$ with $Q_M = Q_0\,\tilde{Q}(1) < 0$, and divide limit $Q_0 = Q(0) > 0$,

$$S(t) \sim -\frac{1}{2}\,t \quad \text{as} \ \ t \to 0, \quad S(t) \sim \tilde{Q}(1)\,(1-t) \ \ \text{as} \ \ t \to 1, \quad S(t) < 0 \ \ \text{for} \ \ 0 < t < 1 \ . \tag{5.5}$$

The third relation supposes there is no divide other than at $R = 0$. If the accumulation is prescribed in the form $Q(R)$, then the zero net flux determines R_M. It follows from (5.4) that $\tilde{\Gamma}(0) = 0$ necessarily.

As a first step the flat bed solution $H_0(R) = \tilde{H}(t) = Y(t)$ say, for $F(R) = \tilde{F}(t) = 0$ is determined as the solution of

$$2\,\tilde{\Gamma}(t)[\tilde{H}(t) + \lambda\,\tilde{H}^3(t)] = [1 + \lambda\,Y^2(t)]\,\frac{dY^2}{dt} = \frac{\kappa}{\lambda}\,S(t) \ , \quad Y(1) = 0 \ , \tag{5.6}$$

which is

$$Y(t) = \left\{\frac{[1+\kappa\,P(t)]^{\frac{1}{2}} - 1}{\lambda}\right\}^{\frac{1}{2}} \ , \tag{5.7}$$

where

$$P(t) = -2\int_t^1 S(y)\,\mathrm{d}y \ > 0 \ \ \text{for} \ \ 0 \le t < 1 \ , \quad P(1) = 0 \ . \tag{5.8}$$

The surface slope is then given by

$$Y'(t) = \frac{1}{2}\,\kappa\,\{\lambda\,[1+\kappa\,P(t)]\}^{-\frac{1}{2}}\left\{[1+\kappa\,P(t)]^{\frac{1}{2}} - 1\right\}^{-\frac{1}{2}}\,S(t) \ , \tag{5.9}$$

with asymptotic expansions

$$t \to 0: \quad Y(t) \sim Y_0 - Y_2\,t^2 \ , \quad Y'(t) \sim -2\,Y_2\,t \ , \quad Y_0 > 0, \quad Y_2 > 0 \ , \tag{5.10}$$

$$t \to 1: \quad Y(t) \sim \left\{-\frac{\kappa\,\tilde{Q}(1)}{2\,\lambda}\right\}^{\frac{1}{2}}(1-t) \ , \quad Y'(t) \sim -\left\{-\frac{\kappa\,\tilde{Q}(1)}{2\,\lambda}\right\}^{\frac{1}{2}} \ , \tag{5.11}$$

where

$$Y_0 = \left\{\frac{[1+\kappa\,P(0)]^{\frac{1}{2}} - 1}{\lambda}\right\}^{\frac{1}{2}}, \quad Y_2 = \left\{\frac{\kappa}{8\,\lambda^{\frac{1}{2}}\,[1+\kappa\,P(0)]^{\frac{1}{2}}\,\{[1+\kappa\,P(0)]^{\frac{1}{2}} - 1\}^{\frac{1}{2}}}\right\} \ . \tag{5.12}$$

The inverse method is to prescribe a thickness distribution $\tilde{\Delta}(t)$ in the form

$$\tilde{\Delta}(t) = Y(t) + Z(t) - Z(1) \ , \quad |Z'(t)|_{\max} = d^{-1} \ , \quad d \ll 1, \tag{5.13}$$

where $d = \epsilon$ corresponds to an order unity derivative in r. From (5.4),

$$\tilde{\Gamma}(t) = \left\{\frac{\kappa\,S(t)}{2\,\lambda\,[\tilde{\Delta}(t) + \lambda\,\tilde{\Delta}^3(t)]}\right\} = O(\Lambda) \ , \quad (0 \le t < 1) \ , \tag{5.14}$$

and with the asymptotic results $(5.5)_2$, and $(5.11)_1$, and choosing $Z(t) - Z(1)$ with the same behaviour as $t \to 1$,

$$Z(t) - Z(1) \sim Z_1\,(1-t) \ , \quad \tilde{\Delta}(t) \sim \Delta_1\,(1-t) \ \ \text{as} \ \ t \to 1 \ , \quad \tilde{\Gamma}(1) = \frac{\kappa\,\tilde{Q}(1)}{2\,\lambda\,\Delta_1} \ . \tag{5.15}$$

The surface slope can therefore be greater than unity, but in general much less than ϵ^{-1} for moderate friction coefficient Λ. Now

$$\tilde{\beta}(t) = R_M\, \beta(R) = \tilde{F}'(t) = \tilde{\Gamma}(t) - Y'(t) - Z'(t) \ , \tag{5.16}$$

which yields a bed slope $\tilde{\beta}(t)$ of order the prescribed large $Z'(t)$, but with opposite sign. The corresponding bed profile is then given by

$$\tilde{F}(t) = -\int_t^1 \tilde{\beta}(y)\,\mathrm{d}y + \tilde{F}(1) \ , \tag{5.17}$$

where the numerical quadrature must be performed with sufficiently small step lengths in regions of large $\tilde{\beta}(t)$, and finally the surface profile by

$$\tilde{H}(t) = \tilde{\Delta}(t) + \tilde{F}(t) \ \text{ or } \ -\int_t^1 \tilde{\Gamma}(y)\,\mathrm{d}y + \tilde{H}(1) \ , \tag{5.18}$$

with $\tilde{F}(1) = \tilde{H}(1)$ a free parameter. Where $|Z'(t)| \ll 1$, $(5.13)_1$ shows that $\tilde{\Delta}'(t) \approx Y'(t)$, and if this applies over some region adjacent to the margin where both $\tilde{\Delta}$ and Y vanish, then $\tilde{\Delta}(t) \approx Y(t)$ there, and hence by (5.4) and (5.6),

$$\tilde{\Gamma}(t) \approx \left\{ \frac{\kappa\, S(t)}{2\,\lambda\,[Y(t) + \lambda\, Y^3(t)]} \right\} \approx Y'(t) \quad \Rightarrow \quad \tilde{H}(t) \approx Y(t) \ , \tag{5.19}$$

and the reduced model solution is approximately a flat bed solution not influenced significantly by large bed slopes elsewhere.

Examples have been constructed for the accumulation function

$$\tilde{Q}(t) = 1 - 2\,t^2 \ , \quad \tilde{Q}(1) = -1 \ , \quad S(t) = -\frac{1}{2}\,t\,(1 - t^2) \ , \tag{5.20}$$

and two prescribed functions $Z(t)$. The first generates a large slope central hump descending to a nearly flat bed at short distance from the divide:

$$Z(t) = Z_0 \exp(-k\,t^2) \ , \quad -Z'(t)_{\max} = Z_0\,(2\,k/e)^{\frac{1}{2}} \ \text{ at } \ t_m = (2\,k)^{-\frac{1}{2}} \ , \tag{5.21}$$

for which $Z(1) = 0$ and the choice $k = \frac{1}{2}\,\mathrm{e}/(Z_0 d)^2$ gives a maximum slope in R of order d^{-1}, and hence $\delta = \epsilon d^{-1}$ in r. The second has a central plateau with a large slope descent to a nearly flat bed at prescribed $t = t_m$:

$$\begin{aligned} Z(t) &= Z_0 \left\{ \frac{\tanh[k\,(1 - t_m)] - \tanh[k\,(t - t_m)]}{\tanh[k\,(1 - t_m)] + \tanh[k\,t_m]} \right\} \ , \quad Z(1) = 0 \ , \\ Z'(t) &= -k\,Z_0 \left\{ \frac{\operatorname{sech}^2[k\,(t - t_m)]}{\tanh[k\,(1 - t_m)] + \tanh[k\,t_m]} \right\} \ , \\ -Z'(t)_{\max} &= \left\{ \frac{k\,Z_0}{\tanh[k\,(1 - t_m)] + \tanh[k\,t_m]} \right\} \ \text{ at } \ t = t_m \ . \end{aligned} \tag{5.22}$$

Since the denominator in the $Z'(t)$ expression (5.22) lies between 1 and 2 for all t_m, choosing $k = 2/(Z_0 d)$ gives a maximum $-Z'(t)$ between d^{-1} and $2\,d^{-1}$. Comparisons with solutions of the full equations are illustrated in Sect. 8.

6 Numerical methods

Focussing on the prescribed temperature theory for steady axi-symmetric flow, a numerical method is required to solve the mass balance (3.2) or (3.3), the radial and vertical equilibrium balances (3.5), and the viscous shear relations (3.6) inside the ice-sheet domain, subject to the conditions on the surface $z = h(r)$ of zero tractions (3.9) and (3.10), and the kinematic condition (3.11), and on the bed $z = f(r)$ the basal kinematic condition (3.17), and the tangential sliding condition (3.18) or no-slip condition $v_s = 0$. In addition there are the conditions of zero surface slope and radial velocity on the axis of symmetry $r = 0$. The surface $z = h(r)$,

and hence the domain, are unknown, to be determined by the additional kinematic condition on the traction-free surface. The two methods adopted both use mappings of the unknown domain onto a fixed domain by a transformation of co-ordinates, and then solve the transformed equations and boundary conditions on the fixed domain by a finite element procedure. Since the basic equations and the mapping relations are non-linear, Newton iteration is used to reduce the problem to a sequence of linear algebraic problems. The first method applies an orthogonal co-ordinate transformation, specifically that developed by Ryskin and Leal (1983), and the second applies a generalisation of the Landau (1950) transformation.

The orthogonal mapping is not explicit, but is determined by two elliptic partial differential equations. Ryskin and Leal (1983) noted that in a Cartesian co-ordinate system the co-ordinate transformation functions both satisfy Laplace's equation, and that the Laplacian can be written in any co-ordinate system once the components of the metric tensor are known. For two dimensional mappings this symmetric tensor has three independent components. In orthogonal co-ordinate systems the off diagonal element must be zero, leaving just two components. A further constraint comes from the fact that the underlying space is Euclidian, which, in two dimensions requires that the Gaussian curvature is zero. This can be satisfied if the ratio of the two diagonal elements of the metric tensor, which are the scale factors, is a function of the co-ordinates only, which is the property adopted here. The original co-ordinates (r, z) are transformed to co-ordinates (ξ, η) by a mapping satisfying the equations Ryskin and Leal (1983), Cliffe et al. (1992),

$$\frac{\partial}{\partial \xi}\left(\frac{1}{\varpi}\frac{\partial r}{\partial \xi}\right)+\frac{\partial}{\partial \eta}\left(\frac{1}{\varpi}\frac{\partial r}{\partial \eta}\right)=0\ ,\quad \frac{\partial}{\partial \xi}\left(\frac{1}{\varpi}\frac{\partial z}{\partial \xi}\right)+\frac{\partial}{\partial \eta}\left(\frac{1}{\varpi}\frac{\partial z}{\partial \eta}\right)=0\ , \tag{6.1}$$

where ϖ is the ratio of the scale factors. Here ϖ is restricted to be a constant. Derivatives with respect to (r, z) are expressed in terms of derivatives with respect to (ξ, η) by

$$\frac{\partial \xi}{\partial r}=\frac{1}{J}\frac{\partial z}{\partial \eta}\ ,\quad \frac{\partial \xi}{\partial z}=-\frac{1}{J}\frac{\partial r}{\partial \eta}\ ,\quad \frac{\partial \eta}{\partial r}=-\frac{1}{J}\frac{\partial z}{\partial \xi}\ ,\quad \frac{\partial \eta}{\partial z}=\frac{1}{J}\frac{\partial z}{\partial \xi}\ , \tag{6.2}$$

where J is the Jacobian of the transformation defined by

$$J=\det\begin{pmatrix}\dfrac{\partial r}{\partial \xi} & \dfrac{\partial r}{\partial \eta}\\ \dfrac{\partial z}{\partial \xi} & \dfrac{\partial z}{\partial \eta}\end{pmatrix}. \tag{6.3}$$

Boundary conditions for the mapping differential equations (6.1) are as follows. On the axis of symmetry

$$r=0\,,\quad \frac{\partial z}{\partial \xi}=0\ . \tag{6.4}$$

On the base

$$z=f(r)\,,\quad \frac{\partial r}{\partial \eta}=-\varpi\frac{\partial z}{\partial \xi}\ , \tag{6.5}$$

where the first relation is a Dirichlet-type condition for $(6.1)_2$ which determines z, and the second relation, which expresses the orthogonality of the η direction to the transformed bed $\eta = 0$, is a Neumann-type boundary condition for $(6.1)_1$ which determines r. On the free surface the kinematic condition (3.11) is applied as a Dirichlet condition for $(6.1)_2$. Orthogonality is used to provide a boundary condition for $(6.1)_1$ along the free surface. This takes the form

$$\frac{\nu_1}{\varpi}\frac{\partial r}{\partial \eta}+\nu_2\varpi\frac{\partial r}{\partial \xi}=-\nu_1\frac{\partial z}{\partial \xi}+\nu_2\frac{\partial z}{\partial \eta}\ , \tag{6.6}$$

where (ν_1, ν_2) is the unit outward pointing normal on the untransformed region. This condition is applied as a Neumann-type boundary condition for $(6.1)_1$.

The Landau transformation Landau (1950), Wheeler and Winters (1989), leaves one co-ordinate direction unchanged and consists of a simple stretching or shortening in the other direction. While this might appear to be simpler than the orthogonal transformation, the transformed conservation equations now have a more complicated form. Here the stretching is chosen so that the transformed surface meets the transformed base with a finite surface slope at the margin. Thus, if the margin radius is r_m,

$$\xi = r/r_m \ , \quad \eta = \frac{z - f(r)}{h(r) - f(r)} \Phi\left(\frac{r}{r_m}\right) \ , \tag{6.7}$$

where η measures the relative height from the bed. The boundary transformations are

$$r = 0: \quad \xi = 0 \, , \quad z = f(r): \quad \eta = 0 \, , \quad z = h(r): \quad \eta = \Phi(\xi) \, , \tag{6.8}$$

and the mapped region is determined by the choice of the function $\Phi(\xi)$, which for this study was taken to be part of an ellipse of similar shape to the ice sheets under study, so that

$$\Phi(\xi) = -1 + 2\sqrt{(1 - 3\xi^2/2)} \ . \tag{6.9}$$

The margin radius r_m and the height of the ice sheet $h(r)$ are determined as part of the solution procedure, essentially from the kinematic condition (3.11) on the ice-sheet surface. If the geometry of the ice sheet is known, then r_m and $h(r)$ are prescribed in advance and the surface accumulation distribution is determined by the solution.

A finite element Galerkin discretisation of the balance, viscous and mapping equations is adopted, based on six-node triangles with quadratic basis functions for all the variables except the pressure for which linear interpolation is used. This method is very similar to the Taylor-Hood method for the Navier-Stokes equations Taylor and Hood (1973), . The method used to solve the discretised equations is based on Newton's method which requires the Jacobian matrix in addition to the equations themselves. The ENTWIFE program used to solve the governing equations has a powerful preprocessing facility, based on the REDUCE Hearn (1991), algebraic manipulation package, which generates the required FORTRAN subroutines. The input to the pre-processor is written in the REDUCE language and consists of the weak forms of the governing equations. In addition, the REDUCE package is also used to evaluate the co-ordinate transformed forms of the equations.

The discrete algebraic non-linear equations are of the form

$$\mathbf{f}(\mathbf{x}, \alpha) = \mathbf{0} \ , \tag{6.10}$$

where $\mathbf{f}$ is a vector function, $\mathbf{x}$ is the vector of all the degrees of freedom in the model, and α is a selected scalar parameter. The problem may have many parameters, but in the method discussed here all but one of them are held fixed for a given set of calculations. Further calculations may be carried out in which a different parameter is varied. Newton's method of solution of the non-linear system applies the iteration procedure

$$\mathbf{x}^{n+1} = \mathbf{x}^n - \left(\frac{\partial \mathbf{f}}{\partial \mathbf{x}}(\mathbf{x}^n)\right)^{-1} \mathbf{f}(\mathbf{x}^n, \alpha) \ , \quad (n = 0, 1, \ldots) \, , \tag{6.11}$$

which is quadratically convergent when the Jacobian matrix $\partial \mathbf{f}/\partial \mathbf{x}$ is continuous and has a bounded inverse in a neighbourhood of the solution. Quadratic convergence means that the number of accurate significant figures in the approximate solution doubles at each iteration and so a calculation rarely needs more that 5 or 6 iterations. Newton's method is guaranteed to converge provided the initial guess $\mathbf{x}^0$ is sufficiently close to the solution, but this condition is not always easy to realise. Suppose now that a solution is known for a particular value α_0 of the parameter, perhaps because a good initial guess is possible, then Euler-Newton continuation can be applied to construct a sequence of solutions for successive small changes in α by adopting the solution for each previous value of α as the initial guess to a Newton iteration for the next value of α. That is,

$$\mathbf{x}^0(\alpha_{k+1}) = \mathbf{x}(\alpha_k) - \left[\frac{\partial \mathbf{f}}{\partial \mathbf{x}}(\mathbf{x}(\alpha_k), \alpha_k)\right]^{-1} \mathbf{f}(\mathbf{x}(\alpha_k), \alpha_k) \ . \tag{6.12}$$

This procedure clearly breaks down if $\partial \mathbf{f}/\partial \mathbf{x}$ becomes singular or nearly singular. The common reason is that there is a turning point on the solution branch, which means that $\mathbf{x}$ is no longer a single valued function of α. Following Keller (1977), this is remedied by introducing a new parameter ζ which is a local approximation to the arclength along the solution branch, so that the solution is clearly a single-valued function of ζ. The new system now has the form

$$\mathbf{f}(\mathbf{x}, \alpha) = \mathbf{0} \ , \quad N(\mathbf{x}, \alpha, \zeta) = 0 \ , \tag{6.13}$$

where $N = 0$ is the defining equation for the arclength parameter. It can be shown Keller (1977), that the extended system (6.13) has a non-singular Jacobian, even at a limit point where $\partial \mathbf{f}/\partial \mathbf{x}$ is singular. This extension of Euler-Newton continuation by Keller Arclength Continuation is the method applied to the present ice-sheet problems.

Before presenting results it is important to confirm the accuracy of the numerical approximation, and to note that a surprisingly large number of elements were required to obtain satisfactory solutions. Using a mesh with too few elements lead to spurious wiggles in the surface accumulation function determined by a solution on a prescribed domain. It is thought that the relatively large aspect ratios of the ice sheets are responsible for this need to have such fine meshes, which makes large demands on computing resources, even in two dimensions. Here the prime aim is to determine accurate solutions to selected problems to establish the range of validity of the *Reduced Model*. A rigorous grid-convergence investigation has therefore been performed, involving successive halving of the element sizes which increases the computation time by a factor 16 at each reduction. The measure chosen to describe each solution is the divide height $h_D(\mu)$ as a function of the mesh size μ, defined as the minimum of the radii of the circular disks required to cover each element. It is expected that the error in the predicted divide height is close to order μ^3 as $\mu \to 0$, for which a good approximation would be

$$h_D(\mu) = h_E + K\mu^3 \ , \tag{6.14}$$

where h_E is the exact value of the divide height, and K is a constant independent of μ. This is tested as follows from three solutions involving two successive halvings of the element sizes. If the approximation (6.14) is accurate, then

$$\frac{h_D(\mu) - h_D(\mu/2)}{h_D(\mu/2) - h_D(\mu/4)} = 8 \ , \quad h_E = \frac{8h_D(\mu/4) - h_D(\mu/2)}{7} \ , \tag{6.15}$$

and good agreement with the ratio 8 would confirm the error magnitude assumption and the accuracy of this estimate for h_E. Table 1a shows the results for one of the examples, for which the defining parameter values are $\bar{T} = -1$, $\Lambda = 100$ and $\epsilon^2 = 2.77 \times 10^{-4}$. For this example the ratio was 8.3, which is sufficiently close to the expected value of 8 to indicate that the error estimate given by (6.14) is good. The estimate for the exact value of h_E is 0.53154, which is compared to the values of the divide height h_D given by the three solutions. It can be seen that, even on the coarsest mesh, the error in the computed divide height is much less than 1%, and is even smaller on the finer meshes, which indicates that very accurate numerical solution have been obtained to the full model equations using the orthogonal mapping technique.

Table 1. Results of the grid convergence study for (a) the orthogonal mapping technique, (b) the modified Landau transformation technique. The effect of grid refinement on the calculated value of the divide height is shown. The linear dimensions of the elements are reduced by a factor of two at each step.

Divide height	Error	Number of nodes	Total number of degrees of freedom	
0.52842	0.00312	3823	26803	
0.53116	0.00038	14834	101458	(a)
0.53149	0.00005	58483	400108	
0.56946	0.00107	3823	26803	
0.57036	0.00017	14834	101458	(b)
0.57051	0.00002	58483	400108	

A similar study was carried out for the modified Landau transformation technique. The parameter values for this case were $\bar{T} = -1$, $\Lambda = 100$ and $\epsilon^2 = 2.77 \times 10^{-4}$. The results are summarised in Table 1b. The estimated factor of 6 is sufficiently close to the expected value of 8 to indicate that the error estimate given by (6.14) is good in this case too. The estimate for the exact value of h_E is 0.57053, which is compared to the values of the divide height h_D given by the three solutions. It can be seen that, even on the coarsest mesh, the error in the computed divide height is much less than 1%, and is even smaller on the finer meshes, which indicates that very accurate numerical solution have been obtained to the full model equations using the modified Landau transformation technique.

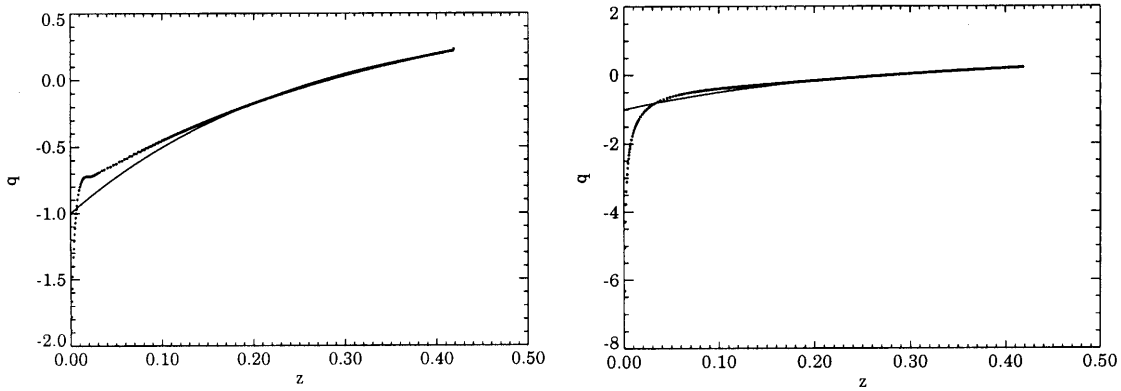

Fig. 1a,b. Computed accumulation/ablation function for full model, with the free surface prescribed to be that given by the solution of the corresponding reduced model. The solid line is the accumulation/ablation function used in the reduced model calculation and the points are the values computed from the full model solution with **a** $\epsilon^2 = 2.77 \times 10^{-6}$ and **b** $\epsilon^2 = 2.77 \times 10^{-4}$

7 Results for flat and small slope beds

Numerical solutions for comparison with the *Reduced Model* small bed slope solutions constructed by Morland (1997) have been determined with the following parameters:

$$d_0 = 2000\,m\,, \quad q_0 = 3.17 \times 10^{-8}\,ms^{-1}\,, \quad D_0 = 3.17 \times 10^{-8}\,s^{-1}\,, \quad a_0 = 1\,,$$
$$\epsilon^2 = 2.776 \times 10^{-6} \text{ and } \epsilon^2 = 2.776 \times 10^{-4}\,, \quad \vartheta = 0.09006\,, \quad \Lambda = 25 \text{ and } \Lambda = 100\,, \qquad (7.1)$$

where the latter friction coefficient essentially describes no-slip except under a small thickness of ice. With this basal sliding law, the *Reduced Model* has errors of order ϵ^2 for a flat bed or maximum bed slope of order ϵ if the hump span is that of the sheet, but of order ϵ if the hump span is that of the sheet thickness. A *Reduced Model* solution is then an accurate solution of the full equations for a flat or very small slope bed, and so provides a test case for the accuracy of a numerical algorithm for the full equations, and a good initial solution to an iteration which builds the topography from a flat bed. However, in the case of no-slip at the bed, the *Reduced Model* assumptions are violated near a margin where the surface slope becomes unbounded, so the solution cannot then be expected to be close to the solution of the full equations near margins. The *Reduced Model* solution is only independent of ϵ in the stretched co-ordinates R, Z, and expression in the physical co-ordinates r, z for comparison with the full equations involves the transformation $R = \epsilon r$. The full equations involve ϵ explicitly through the viscous relations. Recall that an isothermal approximation at a cold temperature should replace a_0 by the much lower rate factor, which determines a much larger ϵ and hence larger errors in the *Reduced Model*.

The first set of tests and comparisons with Morland (1997)'s (1997) solutions were made with an accumulation function

$$q = \frac{1}{2} - \frac{3}{2}\exp(-4h)\,, \quad q(0) = -1\,, \qquad (7.2)$$

which was the small margin ablation example used by Morland (1997), with a snow line $q = 0$ at $h = 549\,m$, and prescribed isothermal and non-uniform temperature distributions

$$\bar{T}_A = -0.25\,(-5\,K)\,, \quad \bar{T}_B = -0.5\,(-10\,K)\,, \quad \bar{T}_C = -1.\,(-20\,K)\,, \qquad (7.3)$$

$$\begin{aligned}\bar{T}_2(r,z) \;=\; & -0.8h(r) + 0.5\,[h(r) - z] \\ & -0.125\left\{[h(r) - f(r)]^2[h(r) - z] - 0.5[h(r) - f(r)][h(r) - z]^2\right\}\,, \end{aligned} \qquad (7.4)$$

following Morland's notation. The small bed slope results were obtained with the orthogonal mapping method, and demonstrate a failure of the continuation procedure with this method. The subsequent moderate and large bed slope results were obtained with the modified Landau transformation.

While the *Reduced Model* solution fails near the margin with no-slip on the bed, and so fails as an initial guess, the surface accumulation q_{red} predicted by the full equations if a *Reduced Model* ice-sheet domain is adopted can be determined for comparison with (7.2). The two accumulation distributions would be very close if the *Reduced Model* is a good approximation. Comparisons are shown in Fig. 1a,b for a flat bed and for two values of ϵ, revealing the expected differences near the margin, but good agreement above relative heights of 0.2. This does not, of course, confirm the accuracy of the algorithm. Now consider a modified surface accumulation

$$\mathbf{u}.\mathbf{n} = -(1-\alpha)q_{\text{red}} - \alpha q \quad , \tag{7.5}$$

where α is called a homotopy parameter. When α is zero the accumulation is the value computed from the full model with the free surface specified to be the same as that obtained from the *Reduced Model*. Thus, if that solution is adopted as an initial guess for an iteration to solve with the kinematic condition given by (7.5), Newton's method should converge very quickly when α is zero, which proved to be the case. Keller-Arclength continuation was then applied to investigate if increasing α in small steps from zero to one would lead to the solution for a no-slip basal boundary condition. However, a turning point was found when α was approximately 0.1 so that there were no solutions, on this solution branch, for greater values of α. For smaller values of α there are two equilibrium solutions, at least one of which is unstable. The existence of this turning point meant that the method will not determine solutions to the full model with a no-slip basal boundary condition, not that a solution does not exist. However, two conclusions can reasonably be drawn from this investigation. Firstly, it is clear that there are significant differences between the reduced and full models when a no-slip basal boundary condition is applied, at least near the margin. Secondly, the full model equations can exhibit multiple equilibrium solutions.

Next consider flat bed problems with the basal sliding law, for which the *Reduced Model* solution is accurate, for the two friction coefficients given in (7.1) and four temperature distributions given in (7.3) and (7.4), making a total of eight different cases. The *Reduced Model* surface $h(r)$ is approximated by a cubic spline for use in the finite element algorithm. The full equations are first solved with this *Reduced Model* surface $h(r)$ as the domain surface, and with a no-slip basal boundary condition which avoids the non-linear sliding law as a first step. This is still a non-linear problem, due to the non-linear viscous relation, and is solved in two stages. First, the viscous relation is linearised by omitting the higher order terms in (2.10), and this problem can always be solved irrespective of the initial guess. Euler-Newton continuation was then used to obtain a solution to the problem with the same fixed free-surface but the full non-linear viscous relation defined by (2.10). This solution was then used as an initial guess for the problem with the sliding-law basal boundary condition. For all the prescribed temperatures the no-slip solution proved to be a sufficiently good initial guess for the sliding law case provided that the shape of the free surface was fixed and the large sliding-law parameter $\Lambda = 100$ was used. Solutions for a sliding-law parameter value of 25 were obtained by continuation in Λ using the solution at $\Lambda = 100$ as the starting point.

The next step takes the surface accumulation q_{red} determined by this solution, uses a cubic spline to express as a function of h, extended beyond the solution range, and applies the continuation method as before to determine the solution, including the actual surface, for the prescribed accumulation (7.2). In all cases the continuation procedure was successful and solutions were obtained to the full problem with the specified accumulation function.

First consider solutions for a flat bed, with the comparisons illustrated by the shape of the free surface and the margin radius and divide height. The margin radius and divide height for the three isothermal cases (7.3) are compared for both values of the friction coefficients with $\epsilon^2 = 2.77 \times 10^{-4}$ in Tables 2a–c, Tables 2a and b show very good agreement between the full-model calculations and the reduced-model calculations for both values of the sliding-law parameter, and similarly, a comparison of the shape of the free surface obtained with the full model and that obtained with the reduced model for the case with $\Lambda = 100$ and $\overline{T} = -0.25$, shown in Fig. 2a, confirms very good agreement. However, Table 2c and Fig. 2b indicates that there is a substantial difference between the full and *Reduced Model* results for the case with $\overline{T} = -1.0$. Repeating the full solutions with $\epsilon^2 = 3.0 \times 10^{-6}$ results in the much better agreements shown in Table 2d and Fig. 2c. This is the anticipated dependence on ϵ at cold temperatures when a_0 in the *Reduced Model* should be much larger than unity, which implies that the ϵ^2 error term is more significant, and the *Reduced Model* is less satisfactory. The good agreement obtained by setting ϵ^2 smaller is artificial, but shows here that the full solution does agree

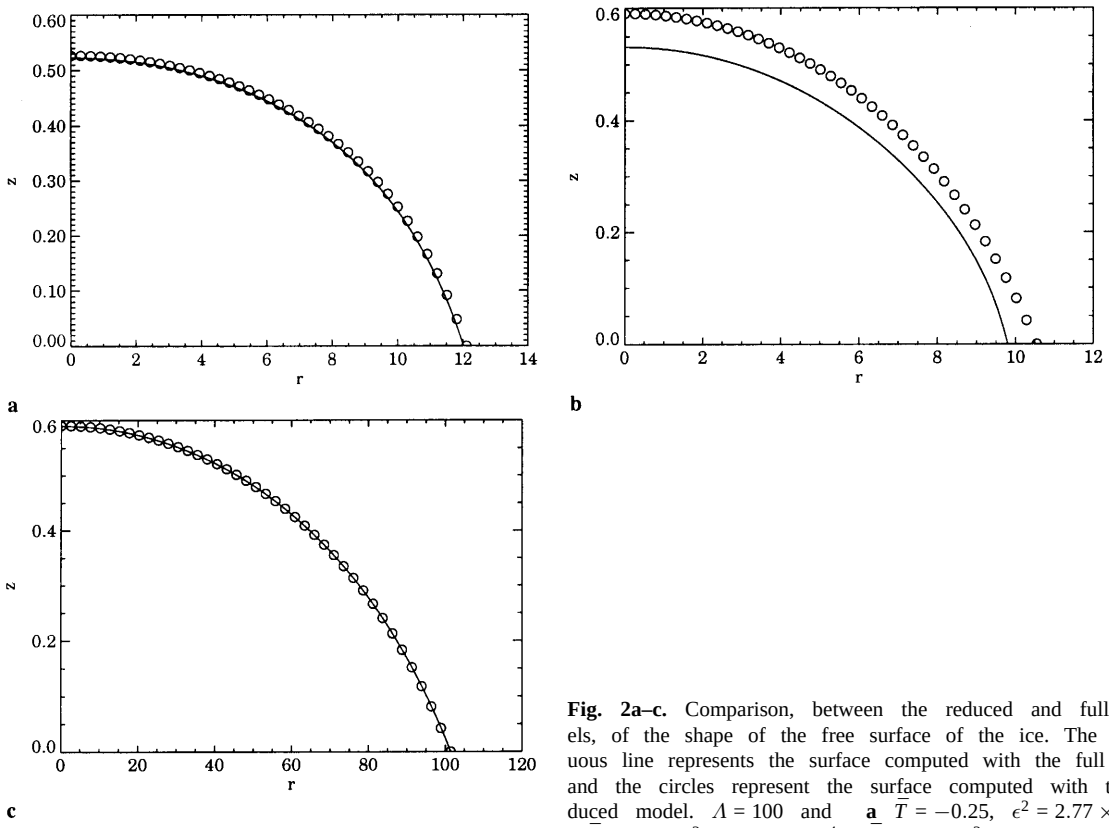

Fig. 2a–c. Comparison, between the reduced and full models, of the shape of the free surface of the ice. The continuous line represents the surface computed with the full model and the circles represent the surface computed with the reduced model. $\Lambda = 100$ and **a** $\bar{T} = -0.25$, $\epsilon^2 = 2.77 \times 10^{-4}$; **b** $\bar{T} = -1.0$, $\epsilon^2 = 2.77 \times 10^{-4}$; **c** $\bar{T} = -1.0$, $\epsilon^2 = 2.77 \times 10^{-6}$.

with the *Reduced Model* solution when ϵ^2 is sufficiently small. Note also that the aspect ratio of the ice sheet is roughly proportional to ϵ^{-1}. The case with the prescribed non-uniform temperature field $\bar{T}_2$, (7.4), also shows a discrepancy between the full and reduced model results, Table 2e, and it is assumed this discrepancy is also related to the prescription of a large cold ice zone which influences the asymptotic magnitudes.

The next stage is to apply Keller Arclength continuation in a homotopy parameter α defining an increasing amplitude bed topography of the form

$$f(r) = 0.1\,\alpha \exp(-20r^2) \ , \tag{7.6}$$

for which Morland (1997) gives *Reduced Model* solutions. Starting from the flat bed solution to the problem with the temperature field prescribed by (7.4), Keller Arclength continuation is applied to successive small increases of α. However, a turning point was found for a value of α of about 0.15, suggesting at first that there is no equilibrium solution to the ice-sheet problem when the height of the hump is too large. On a closer examination of the results it was seen that two solutions computed for values of α less than 0.15 were not physically different, but corresponded to the same solution with two different co-ordinate transformations. This clearly shows that the co-ordinate transformation equations can have multiple solutions, and not allow continuation to larger values of α. Repeating the calculations on two finer meshes, halving the linear dimensions of the elements in each case, a turning point was reached at values of α of approximately 0.22 and 0.26 respectively; that is, at increasing values of α as the mesh is refined, indicating that its presence might well be due to the discretisation. However, the computational times for the finest mesh were so long that further mesh refinement was impractical. This non-uniqueness of the orthogonal co-ordinate transformation with the continuation method indicates that it is not suitable to determine solutions of the full ice-sheet equations when a bed topography amplitude is increased. Before the turning point, while bed slopes are still small, comparisons with the *Reduced Model* solutions are good, as expected, as confirmed by Fig. 3a,b, which show the variation of divide height and margin radius with hump height as α is increased.

Table 2. Comparison of computed values of the margin and divide height obtained with the reduced and full models.

Λ	R_M (Reduced)	R_M (Full)	H_D (Reduced)	H_D (Full)		
100	12.11	12.01	0.527	0.522	(a)	$\bar{T} = -0.25$
25	21.68	21.59	0.573	0.566		$\epsilon^2 = 2.77 \times 10^{-4}$
100	11.14	10.94	0.559	0.545	(b)	$\bar{T} = -0.5$
25	21.11	20.81	0.589	0.570		$\epsilon^2 = 2.77 \times 10^{-4}$
100	10.54	9.80	0.590	0.531	(c)	$\bar{T} = -1.0$
25	20.79	19.17	0.600	0.529		$\epsilon^2 = 2.77 \times 10^{-4}$
100	101.43	101.33	0.590	0.590	(d)	$\bar{T} = -1.0$
100	101.43	101.33	0.590	0.590	(d)	$\bar{T} = -1.0$
						$\epsilon^2 = 3.0 \times 10^{-6}$
100	13.37	12.06	0.529	0.523	(e)	$\bar{T} = \bar{T}_2$
						$\epsilon^2 = 2.77 \times 10^{-4}$

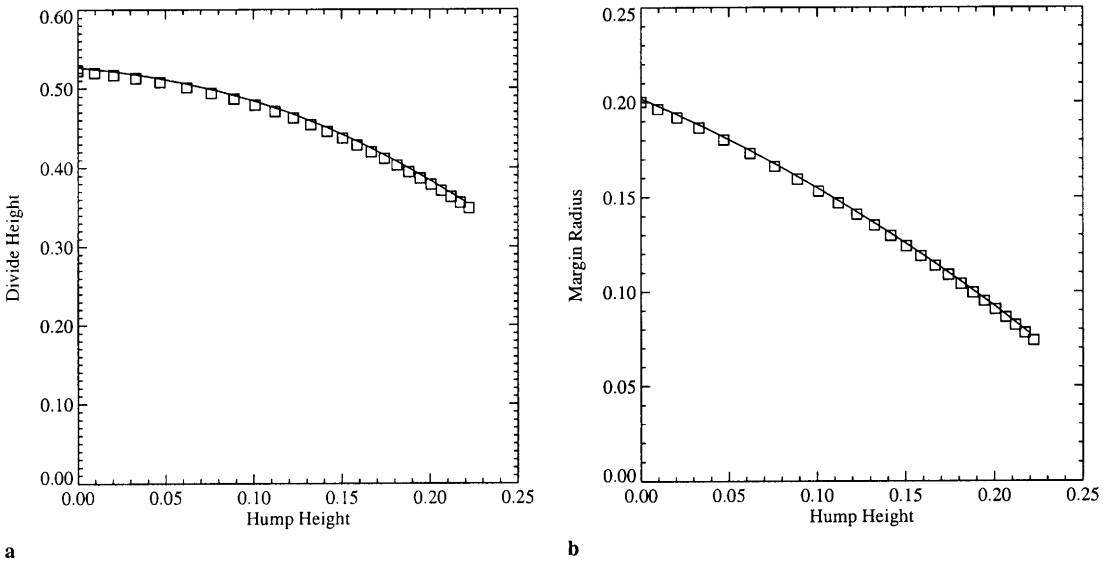

Fig. 3a,b. Comparison, between the reduced and full models, of the variation of **a** divide height, and **b** margin radius with hump height. The continuous line indicate the full model results and the squares indicate the reduced model results.

8 Results for moderate and large slope beds

While the orthogonal co-ordinate transformation produces solutions to the full ice-sheet equations which agree well with the *Reduced Model* when the parameter ϵ is sufficiently small and the bed topography is nearly flat, it was demonstrated that continuation fails to yield a solution when the bed topography amplitude, and associated slope, are increased beyond modest levels. This is surprising in view of the fact that similar methods have been applied very successfully to free-surface fluid dynamics problems that appear to be more difficult than the present ice-sheet problems. In particular, the method has determined a rapidly undulating free-surface in a channel flow which correlates accurately with experimental data Cliffe et al. (1992), . An alternative modified Landau transformation, described in Sect. 6, has therefore been investigated. When applied to prescribed surfaces it has similar accuracy to the orthogonal transformation method, but attempts to compute a free surface by continuation using the kinematic surface condition (3.11) directly resulted in an unstable oscillation of the shape of the free surface that is clearly linked to the element size. However, further investigations of this phenomenon Cliffe (2000), showed how the application of the surface condition (3.11) in the non-standard form

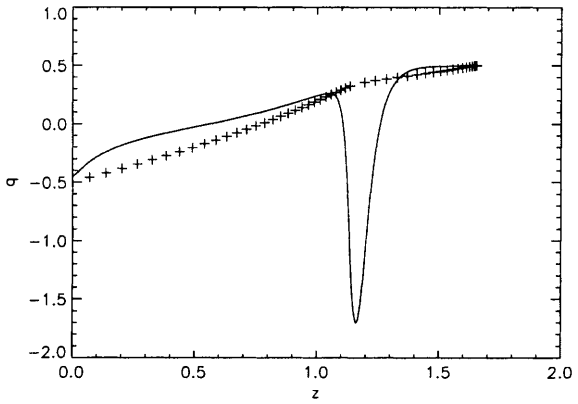

Fig. 4. Computed accumulation/ablation function for full model for flow over an axi-symmetric hump with moderate bed slope. The free surface is prescribed to be that given by the solution of the corresponding reduced model. The + signs indicate the accumulation/ablation function used in the reduced model calculation and the continuous line indicates the accumulation/ablation function computed with the full model.

$$\frac{\partial}{\partial r}\left(u\frac{dh}{dr}\right) - \frac{\partial \tilde{q}}{\partial h}\frac{dh}{dr} = \frac{\partial w}{\partial r} \tag{8.1}$$

eliminated this instability. This application has allowed successful solutions of the ice-sheet problems.

Consider first an example of moderate slope bed topography for which the *Reduced Model* solution was constructed by the inverse method described in Sect. 5. The maximum slope depends on the value of the parameters d and ϵ, and in the present calculation with $d = 0.1$ and $\epsilon = 0.03$ the maximum slope is approximately 0.3, for which the local error is $\delta^2 = 0.09$. By prescribing the free surface as that determined by the *Reduced Model* solution, the solution of the full equations determines a normal surface velocity which defines the surface accumulation distribution necessary for this full solution. This is compared with the prescribed accumulation distribution in Fig. 4, both shown as functions of the *Reduced Model* surface height h. It is seen that over most of the values of h there are not major differences between the two accumulation functions, but in a relatively small range of h corresponding to that part of the ice sheet over a basal region near the 'moderate bed slope', there is a dramatic difference between the two functions. This indicates that there are large differences between the full and *Reduced Model* solutions in the region of the bed slope. However, since the velocity field is sensitive to the shape of the surface, it is possible that a relatively small adjustment to the surface shape in the region of the slope might result in a significant change in the accumulation function. Similar comparisons have been obtained by Morland and Draghicescu (1998) in a linearly viscous plane-flow treatment by complex variable methods. The actual differences, and therefore the extent of the validity of the *Reduced Model*, require the determination of the free surface which solves the full boundary-value problem.

Finally, a series of calculations was carried out, using the modified Landau transformation, in which the bed topography and surface ablation/accumulation were prescribed and the surface shape was computed. The bed topography and surface accumulation were constructed for the *Reduced Model* using the inverse method described in Sect. 5 with $d = 0.1$ In the full model numerical calculations the parameter ϵ was varied from 0.03 to 0.1. The *Reduced Model* solution is, of course, independent of ϵ. However, changing ϵ corresponds to changing the aspect ratio of the ice sheet and the maximum slope δ of the bed topography. The maximum slope of the bed for $\epsilon = 0.03$ is approximately 0.3, and for $\epsilon = 0.1$ is approximately unity.

A comparison of the full and *Reduced Model* solutions is shown in Fig. 5. The agreement for the case with $\epsilon = 0.03$, corresponding to a maximum gradient of 0.3, in spite of the expected local error 0.09, is clearly good. It is interesting to note that this is essentially the same case as that reported earlier in which the surface shape was prescribed and the accumulation rate was computed using the full model. It is evident that a relatively small adjustment in the surface shape is sufficient to change the surface velocities so that the kinematic condition is satisfied. This also illustrates the fact that the velocity field in the ice is sensitive to changes in the shape of the ice-sheet surface.

It is also clear from Fig. 5 that the errors in the *Reduced Model* solution increase as the value of ϵ, and hence δ, increase. Since the *Reduced Model* error is at greatest $O(\epsilon)$, we suggest that the main reason for this is the increase in the maximum gradient of the bed topography, and not simply the neglect of higher order

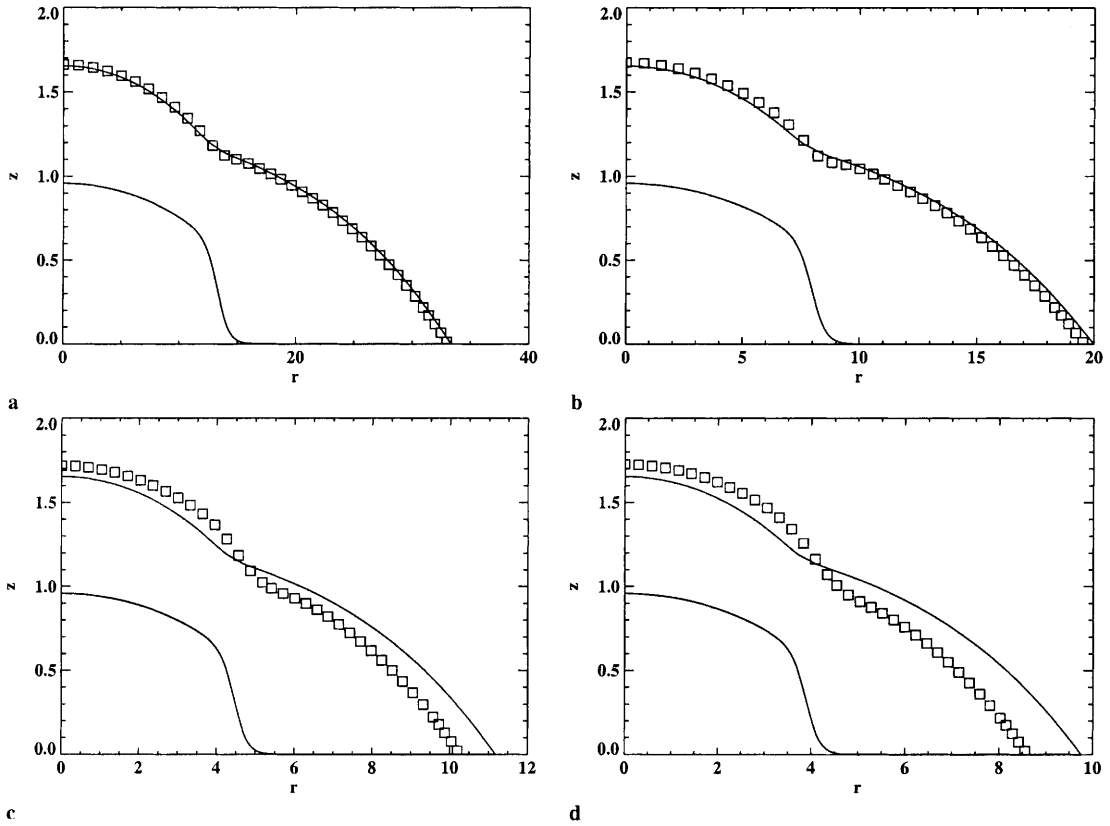

Fig. 5a–d. Comparison of the surface profiles for the full (*squares*) and reduced model (*solid line*) solutions for ϵ^2 = **a** 9×10^{-4}, **b** 2.5×10^{-3}, **c** 8×10^{-3} and **d** $\times 10^{-2}$. The bed topography is also shown as a thick line.

terms in ϵ. For moderate bed slopes the *Reduced Model* gives reasonably accurate solutions for the ice-sheet surface.

Conclusions

A successful method for solving the full equations for axi-symmetric steady isothermal flow of an ice sheet on a bed with significant bed topography has been developed. A sequence of comparisons with solutions given by the *Reduced Model* approximate equations, justified only for very small bed topography, demonstrate that indeed the *Reduced Model* solutions have increasing error as the bed slope increases. In particular while the ice-sheet surface determined by the *Reduced Model* may have only a moderate error at large bed slopes, the errors in the velocity field are significant. In reality ice has a temperature-dependent viscosity, and an ice sheet has a non-uniform temperature field determined by a thermo-mechanically coupled energy balance with significant heat advection. Errors in the velocity field must therefore have a wider impact on the complete flow and geometry of the sheet. This conclusion must question the validity of wider *Reduced Model* simulations of ice-sheet evoluti on, which are the current practice in climate studies.

Acknowledgements. This study was funded by United Kingdom Nirex Limited under the Nirex Safety Assessment Research Programme (NSARP). The authors are grateful for the review of the paper by the NSARP Biosphere Programme Manager, Dr M C Thorne (AEA Technology).

References

1. Cliffe KA (2000) A Numerical Method for Solving the Equations Governing the Flow of Ice. In Preparation.
2. Cliffe KA, Tavener SJ, Wheeler AA (1992) An Orthogonal Mapping Technique for the Computation of a Viscous Free-Surface Flow. Int. J. Numer. Methods Fluids, 155: 1243–1258
3. Glen JW (1955) The Creep of Polycrystalline Ice. Proc. R. Soc. Lond. A, 228: 519–538
4. Hearn AC (1991) REDUCE User's Manual Version 3.4. Rand Publication CP78, Santa Monica
5. Hutter K (1983) Theoretical Glaciology. Reidel
6. Hutter K, Yakowitz S, Szidarovsky F (1987) Coupled Thermomechanical Response of an Axi-symmetric Cold Ice Sheet. Water Resources Research, 23: 1327–1339
7. Huybrechts PA, Payne AJ (1996) The EISMINT benchmarks for testing ice-sheet models. Annals Glaciology, 23: 1–14
8. Keller HB (1977) Numerical Solutions of Bifurcation and Nonlinear Eigenvalue Problems. In: Rabinowitz PH (ed.) Applications of Bifurcation Theory, pages 359–384, New York: Academic Press 1977
9. Landau HG (1950) Heat Conduction in a Melting Solid. Q. Appl. Math., 8: 81–94
10. Mangeney A, Califano F, Hutter K (1997) A Numerical Study of Anisotropic, Low Reynolds Number, Free Surface Flow for Ice Sheet Modelling. J. Geophys. Res., 102: 22749–22764
11. Mellor M, Testa R (1969) Effects of Temperature on the Creep of Ice. J. Glaciology, 8: 131–145
12. Morland LW (1984) Thermomechanical Balances of Ice Sheet Flows. Geophys. Astrophys. Fluid Dyn., 29: 237–266
13. Morland LW (1993) The Flow of Ice Sheets and Ice Shelves, CISM Lectures 1992, no. 337. In: Hutter K (ed.) Continuum Mechanics in Environmental Sciences and Geophysics, pages 402–446, Berlin: Springer 1993
14. Morland LW (1997) Radially Symmetric Ice Sheet Flow. Phil. Trans. R. Soc. Lond. A, 355: 1873–1904
15. Morland L, Draghicescu A (1998) Steady Plane Isothermal Linearly Viscous Flow of Ice Sheets on Beds with Large Slope Topography. Environmetrics, 9: 459–492
16. Morland LW, Johnson IR (1980) Steady Motion of Ice Sheets. J. Glaciology, 25: 229–246
17. Morland LW, Johnson IR (1982) Effects of Bed Inclination and Topography on Steady Isothermal Ice Sheets. J. Glaciology, 28: 71–90
18. Morland LW, Smith GD (1984) Influence of Non-uniform Temperature Distribution on the Steady Motion of Ice Sheets. J. Fluid Mech., 140: 113–133
19. Ryskin G, Leal LG (1983) Orthogonal Mapping. J. Comp. Phys., 50: 71–100
20. Smith GD, Morland LW (1981) Viscous Relations for the Steady Creep of Polycrystaline Ice. Cold. Reg. Sci. Tech., 5: 141–150
21. Taylor C, Hood P (1973) A Numerical Solution of the Navier-Stokes Equations Using the Finite-Element Technique. Computers and Fluids, 1: 73–100
22. Wheeler AA, Winters KH (1989) On a Finite Element Method for the Calculation of Steady Cellular Interfaces in the One-Sided Model of Solidification. Comm. Applied Numer. Methods, 5: 309–320